Remote Sensing of Environment 137 (2013) 274–287

Contents lists available at SciVerse ScienceDirect

Remote Sensing of Environment

journal homepage: www.elsevier.com/locate/rse

Taking stock of circumboreal forest carbon with ground measurements, airborne and spaceborne LiDAR☆

Christopher S.R. Neigh [a,*], Ross F. Nelson [a], K. Jon Ranson [a], Hank A. Margolis [b], Paul M. Montesano [a,c,d], Guoqing Sun [a,d], Viacheslav Kharuk [e], Erik Næsset [f], Michael A. Wulder [g], Hans-Erik Andersen [h]

[a] Biospheric Sciences Laboratory, Code 618, NASA Goddard Space Flight Center, Greenbelt, MD 20771, USA
[b] Université Laval, Centre d'étude de la forêt, Quebec, Quebec G1V 0A6, Canada
[c] Sigma Space Corporation, 4600 Forbes Blvd, Lanham, MD 20706, USA
[d] University of Maryland, Department of Geographical Sciences, College Park, MD 20742, USA
[e] Russian Academy of Sciences, Sukachev Institute of Forest, Krasnoyarsk 660036, Russia
[f] Department of Ecology and Natural Resource Management, Norwegian University of Life Sciences, P.O. Box 5003, NO-1432 Ås, Norway
[g] Canadian Forest Service (Pacific Forestry Center), Natural Resources Canada, 506 West Burnside Rd., Victoria, BC V82Z 1M5, Canada
[h] U.S. Forest Service, Pacific Northwest Research Station, University of Washington, Anderson Hall, Room 207, P.O. Box 352100, Seattle, WA 98195-2100, USA

ARTICLE INFO

Article history:
Received 25 January 2013
Received in revised form 18 June 2013
Accepted 24 June 2013
Available online 29 July 2013

Keywords:
LiDAR
Biomass
Carbon
Boreal forest

ABSTRACT

The boreal forest accounts for one-third of global forests, but remains largely inaccessible to ground-based measurements and monitoring. It contains large quantities of carbon in its vegetation and soils, and research suggests that it will be subject to increasingly severe climate-driven disturbance. We employ a suite of ground-, airborne- and space-based measurement techniques to derive the first satellite LiDAR-based estimates of aboveground carbon for the entire circumboreal forest biome. Incorporating these inventory techniques with uncertainty analysis, we estimate total aboveground carbon of 38 ± 3.1 Pg. This boreal forest carbon is mostly concentrated from 50 to 55° N in eastern Canada and from 55 to 60° N in eastern Eurasia. Both of these regions are expected to warm >3 °C by 2100, and monitoring the effects of warming on these stocks is important to understanding its future carbon balance. Our maps establish a baseline for future quantification of circumboreal carbon and the described technique should provide a robust method for future monitoring of the spatial and temporal changes of the aboveground carbon content.

1. Introduction

The boreal forest biome covers 12.5 ± 1.5 million square kilometers (km^2) (Dixon et al., 1994; Wulder, Campbell, White, Flannigan, & Campbell, 2007) accounting for ~27% of the global forested area, and stores a vast quantity of carbon in its vegetation and soils (Pan et al., 2011). This biome has experienced the greatest magnitude of warming of all biomes over recent decades with a 1–3 °C, or more, increase in seasonal surface air temperature (Hansen et al., 2006), and has experienced the greatest proportion of forest cover lost of all forested biomes from 2000 to 2005 (Hansen, Stehman, & Potapov, 2010). There are large uncertainties in estimates of the size and spatial distribution of boreal forest carbon (C) stocks, and we do not know how it will respond to future warming, forcings and feedbacks (Grosse et al., 2011; Tchebakova, Parfenova, & Soja, 2011). Underlying this biome is rich organic soil C containing 50% of the total global soil pool (1642 Pg C) that has accumulated over the past 10,000+ years following glacial retreat, with 88% of it locked in a permafrost C pool (Tarnocai et al., 2009). Warming-induced thawing of permafrost could enhance decomposition and increase C flux to the atmosphere, negating the long-term sink this biome has supported for centuries (Canadell et al., 2007). To date, the spatial distribution of aboveground C stock throughout this biome has not been characterized with satellite LiDAR (Light Detection and Ranging) measurements. Furthermore, there is no universally recognized definition of the boreal forest, and this can lead to errors in C stock estimates

* Corresponding author. Tel.: +1 301 614 6681.
E-mail address: Christopher.S.Neigh@nasa.gov (C.S.R. Neigh).

0034-4257/$ – see front matter © 2013 The Authors. Published by Elsevier Inc. All rights reserved.
http://dx.doi.org/10.1016/j.rse.2013.06.019

(Houghton et al., 2007). To reduce uncertainties in the global C balance, we must improve our characterization of C stocks in the boreal forest. This is key to improving our understanding of how this biome may change with warming climate.

The boreal forest biome extends in a circumpolar band 13,400 km in length around the Northern Hemisphere roughly between 45° N and 70° N. It is bound by tundra to the north and by temperate deciduous forests or savanna/prairie/steppes to the south. Coniferous species of spruce, pine, and fir as well as deciduous larches, birches, alders, and aspens dominate vegetation cover. Forest fires and insect outbreaks are the dominant agents of disturbance and the size of these events dwarfs those in other biomes because they are typically not suppressed as most do not impact population centers (Stocks et al., 2001). Harvest occurs primarily in southern portions of the boreal forest due to higher productivity and limited access in the north. All of these disturbances have had a major impact on C throughout Canada (Kurz & Apps, 1999) with similar impacts during the 1990s in Siberia (Kharuk, Ranson, & Dvinskaya, 2008). Recently in western North America, mountain pine beetle outbreaks (*Dendroctonus ponderosae*), facilitated by fire suppression and changes in climate, have resulted in widespread tree mortality that has markedly reduced C stocks present in the impacted forests (Kurz et al., 2008). In eastern Canada, outbreaks of spruce budworm (*Choristonneura fumiferana* Clem.) and hemlock looper (*Lambdina fiscellaria* Guen.) could potentially negate the forest C sink (Dymond et al., 2010). The most recent catastrophic insect outbreak in northern Eurasia occurred in the mid 1990s (Kharuk, Ranson, Kozuhovskaya, Kondakov, & Pestunov, 2004). Climate warming may have already induced more fire disturbance and frequent insect outbreaks extending the zone northward, and may have even begun a biome shift into the taiga–tundra transition zone (Ropars & Boudreau, 2012). Increased productivity (Goetz, Mack, Gurney, Randerson, & Houghton, 2007) and increased woody vegetation cover containing more C have already been observed in the high arctic tundra (Ropars & Boudreau, 2012). The vast area of the boreal forest, its large C stocks, and the rapid change that is occurring, all provide a rationale for production of a baseline map of C stocks throughout the biome. Here we report aboveground C total mass and density for 2005, with estimates of uncertainty, developed using model-based estimators (Ståhl et al., 2011), by leveraging forest structure data obtained by the Geoscience Laser Altimeter System (GLAS) onboard the Ice, Cloud, and land Elevation Satellite (ICESat). An underlying assumption of these estimators is that the regression models that relate ground-based estimates of biomass to airborne LiDAR or satellite LiDAR measurements must be correctly specified for the area of interest, otherwise estimates may be biased. In addition, descriptions of procedures which may be used to measure regional C stocks in remote and inaccessible regions of the boreal forest where little information exists are provided.

2. Data and methods

Spaceborne LiDAR remote sensing provides an opportunity to conduct forest C assessments because of the capability for repeated measurements over large areas of interest. The launch of the GLAS sensor onboard ICESat in January 2003 offered the first opportunity to evaluate the potential of a spaceborne LiDAR for measuring structural properties of the boreal forest. ICESat stopped collecting data in 2009, although it has provided a wealth of data that was used to produce global forest height maps (Lefsky, 2010; Los et al., 2012; Simard, Pinto, Fisher, & Baccini, 2011). GLAS estimates have also been used for large area stand volume and/or C in the tropics (Baccini et al., 2012; Saatchi et al., 2011), North America (Nelson, Boudreau, et al., 2009), and Siberia (Nelson, Ranson, et al., 2009). Other studies have related satellite-derived normalized difference vegetation index (NDVI) data (Dong et al., 2003) and spaceborne synthetic aperture radar (SAR) (Santoro et al., 2011) to ground-based estimates of biomass. Our study used a hierarchical sampling approach to estimate treed circumboreal forest carbon (C); specifically from total aboveground live dry biomass density (AGB); we approximate C to be 50% of AGB (Houghton et al., 2000). This hierarchical scheme related AGB data collected on ground plots to airborne and spaceborne LiDAR measurements. The goal was to develop model-based estimates of boreal forest AGB for land cover strata within ecoregions for five circumpolar regions — Alaska, western Canada, eastern Canada, western Eurasia, and eastern Eurasia. We utilized two similar approaches in North America and Eurasia. We based these methods on available data and lessons learned from prior investigations using GLAS-based models to predict AGB and C stock. These data have been used in two smaller regional studies in 2004 for a portion of Siberia (Ranson, Sun, Kovacs, & Kharuk, 2004a,b), in 2005–2006 for southern Norway (Næsset et al., 2011; Ståhl et al., 2011), and in 2005 for the province of Quebec in Canada (Boudreau et al., 2008; Nelson, Boudreau, et al., 2009). We supplemented existing ground and airborne data collected in prior studies, with new field measurements and additional airborne LiDAR data.

2.1. Ground plot data

The Canadian Forest Service (CFS) provided access to relevant plot data holdings and liaised with provincial and territorial forest resource management agencies to obtain access to geo-located ground plots in Canadian boreal ecoregions. Based on the large area and number of jurisdictions involved, numerous individual researchers, provincial foresters, and industrial foresters measured these plots. Field measurements used in this study were collected in Northwest Territories (2006–2008), Saskatchewan (2004–2006), Ontario (2006–2007), and Quebec (2001–2004). The CFS has established species-specific, national-level equations (Lambert, Ung, & Raulier, 2005) that we used in this study to convert ground plot measurements to AGB.

In Alaska, we accessed 361 geo-located ground plots measured by the following U.S. organizations: Forest Service — Kenai Peninsula; Department of Defense — military installations near Fairbanks; and the National Park Service — near Denali N.P., Wrangell — St. Elias N.P., and Yukon — Charley Rivers National Preserve from 2005 to 2007. United States Forest Service (USFS) in conjunction with a related study compiled the plot locations and associated ground measurements.

Field data were collected with a variety of techniques across Eurasia in 2007, 2008 and 2010. In western Eurasia 201 ground plots were collected in a 960 km^2 area in south-eastern Norway. More information about how these data were collected can be found in Næsset et al. (2011). In southern Siberia and northeast China, 322 fixed area ground plots were established on GLAS pulse centroids using a Trimble GeoXT differential global position system (dGPS). Of these 322 plots, we ultimately used 55 to establish the eastern Eurasian model relating ground estimates of biomass to GLAS measurements. We discarded a majority of the unused ground plots either because the associated GLAS measurements were outside of our acceptable temporal window or because of insufficient signal. The 55 ground plots allowed us to develop predictive models that related ground-measured biomass to GLAS measurements. Before field data collection, GLAS waveforms were visually examined to select for a strong vegetation signature for potential field measurement, not confounded by clouds or slope. We selected GLAS shots for which data suggested a strong vertical signature of vegetation. In northern Siberia, sample plots were collected along the Kochechum River in 2007 and the Kotuykan River in 2008. Both expeditions included transport into the field by helicopter, then boat transport down-river accessing GLAS shots within 2–3 km of the river for ~2-week long expeditions. During the summer of 2010, GLAS shot locations were accessed by four-wheel drive vehicle near Chylum-Ket River region in the western plains of Siberia.

We adopted a two-step procedure to calculate biomass at GLAS shot centroids. Field measurements and observations, made in single radius (circular) plots of 10 or 15 m consisted of: 1) tree species and diameter at breast height (DBH), ±0.1 cm, for all trees ≥ 3.0 cm in the entire plot; and 2) a sampling of tree height measurements from small, medium, and tall trees for each plot to characterize the range of heights. In general, a 10 m radius plot was employed in dense southern stands (between 50° and 60° N) and a 15 m radius plot was employed in sparser stands above 60° N latitude. We were able to collect field data across a broad area of Siberia; but we acknowledge a notable geographic gap in our Eastern Hemisphere ground measurements. Access is limited to these forests due to cost and available field personnel to collect measurements over vast remote areas, particularly in the Russian Federation Far East.

2.2. Airborne LiDAR data

2.2.1. PALS

The Portable Airborne Laser System (PALS; Nelson, Parker, & Hom, 2003) instrument serves as an intermediate sampling tool in North America to extend the spatially limited Canadian National Forest Inventory (NFI) and the U.S. Forest Inventory Analysis (FIA) ground measurements to the continental-scale GLAS observations. The system records the LiDAR range/amplitude data stream interleaved with dGPS location information, and also records a dGPS-annotated video of targets overflown (Nelson et al., 2003). The airborne system has been used to measure forest height and canopy closure along GLAS orbital transects 1000s of km in length. The nominal flight profile for the Alaska and Canada airborne laser data collection required the pilots to fly ~150 m–200 m above-ground-level (AGL) at a speed of approximately 97 kn (~180 km h^{-1} or 50 m s^{-1}). Eastern Canada data (Quebec) were collected in the summer 2005, central (Ontario) and western Canada (Northwest Territories and Saskatchewan) were collected in the summer of 2009, and Alaska data were collected in the summer of 2008. Data were typically acquired at 333 Hz, yielding an effective along-track post spacing of 15 cm. The size of the laser spot at target was ~45 cm, so there was (intentionally) significant oversampling along track. Post-flight processing was done to identify ground returns. A spline was fit to the ground points to define a ground line. Once the ground line was identified, canopy height could be calculated for every pulse. The PALS data stream contains ranging information that can be used to calculate canopy height, top-of-canopy height variation, and canopy closure (see Nelson et al., 2003, Fig. 1).

2.2.2. ALTM

In Southeast Norway airborne data were collected with an Optech Airborne Laser Terrain Mapper (ALTM) 3100 system flying at an altitude of ~1850 m at a speed of approximately 145 kn (~270 km h^{-1} or 75 m s^{-1}). Data were acquired in the summer of 2005 with a pulse repetition frequency of 50 kHz, with a scan frequency of 71 Hz, resulting in a point density on the ground of approximately 0.7 m^2. The maximum scan angle was 15° but pulses emitted at an angle > 13° were discarded during subsequent data processing. These airborne data served as an intermediate sampling tool to extend spatially limited survey plots. More information about how the data were processed can be found in Næsset et al. (2011).

2.3. ICESat–GLAS LiDAR data

The Ice, Cloud, and land Elevation Satellite (ICESaT) was launched in January 2003 with the GLAS instrument on-board. We accessed and processed GLAS GLA-01 (waveform) and GLA-14 (land) data distributed by the National Aeronautical and Space Administration (NASA) Goddard Space Flight Center (GSFC) (http://reverb.echo.nasa.gov). We used the satellite data as a sampling tool to understand forest vertical structure (Harding & Carabajal, 2005; Sun, Ranson, Kimes, Blair, & Kovacs, 2008). GLAS carried three lasers that were used sequentially to collect measurements on 33–55 day sub-cycles from January 2003 through October 2009. In our study, we used GLAS pulses from L2a, L3a, L3c, and L3f from the early fall of 2003 through late spring of 2006 (Table 1).

Table 1
ICESAT–GLAS periods of data used in this study listed by laser acquisition.

Laser identifier	Start date (mm-dd-yr)	End date (mm-dd-yr)	Pulse footprint size
L2a	09-24-03	10-15-03	95 × 52 m
L3a	10-03-04	10-15-04	61 × 47 m
L3c	06-08-05	06-13-05	61 × 47 m
L3f	06-08-06	06-26-06	61 × 47 m

Cycles of data were acquired in June and September–October. Our study focused on within-growing-season data, and when available leaf-on conditions. The lasers of GLAS had a slightly elliptical ground pulse spots occurring every 172 m along the ground track of the spacecraft (Abshire et al., 2005). GLAS is a waveform instrument (Harding & Carabajal, 2005), unlike PALS, which records a first–last return range measurement from aircraft to target for each pulse. GLAS records the brightness of the 1.064 μm, near-infrared return in one-nanosecond increments as the pulse traverses from the top of the target to the ground. Over trees, the sequential returns recorded for a single pulse provide an initial return from the top of the canopy. Through sequential secondary returns in 15 cm vertical bins, they also provide ranging measurements to sub-canopy layers and the ground as the pulse traverses vertically from top to bottom (Ranson et al., 2004a).

Each individual waveform can be analyzed to extract a number of measurements related to the biophysical characteristics of the forest canopy (Yong, Sun, & Li, 2004). Such measurements include total canopy height, height to sub canopy layers, heights associated with different percentages of pulse energy return, height of median energy (HOME), canopy density (if assumptions are made concerning ground/canopy reflectivity ratio), and canopy height variability (Sun et al., 2008; Yong et al., 2004). These structurally related measurements, in turn, can be related to forest biophysical characteristics of interest such as basal area, timber volume, aboveground biomass, and C stocks (Lefsky, Harding, Parker, Acker, & Gower, 2002; Sun et al., 2008).

2.4. ASTER GDEM data

GLAS pulse interactions with vegetation on topography with a significant slope can result in pulse broadening, which confounds the interpretation of the influence of the vegetation alone on the waveform (Harding & Carabajal, 2005). We processed Advanced Spaceborne Thermal Emission and Reflection (ASTER) Global Digital Elevation Map (GDEM) Version 1 (V1) data to reduce the impact of pulse broadening. All poor quality GLAS pulses in North America, western Eurasia and eastern Eurasia were eliminated using techniques similar to those described by Lefsky, Keller, Pang, de Camargo, and Hunter (2007) using the thresholds provided in Table 2.

The Ministry of Economy, Trade, and Industry (METI) of Japan and NASA jointly constructed the GDEM V1 data. Multiple along-track stereo acquisitions were processed from the near-infrared spectral band and its nadir-viewing and backward-viewing telescopes with a base-to-height ratio of 0.6 at 15 m resolution. The GDEM data, dating back to 1999, covers 98% of the Earth's land surface in ~1° tiles (60 × 60 km ground area). ASTER GDEM V1 data were selected over Shuttle Radar Topography Mission (SRTM) data because of the higher resolution of the product (30 m vs. 90 m), and because of the near global coverage. SRTM data are

Table 2
GLAS and ASTER GDEM metrics and valid ranges used to identify and exclude poor quality laser pulses.

Metric	Valid range
AGB	<500
wflen	0 < 80
meanH, qmch, medH, Centroid, h_{14}, h_{100}	−10 < 50
satndx	≤2
ASTER GDEM slope	<20°

Variable definitions:

AGB	above ground live dry biomass, in megagrams per hectare
wflen	total vertical extent of the GLAS waveform from signal start to signal end
meanH	mean canopy height (Lefsky, Harding, Cohen, Parker, & Shugart, 1999)
qmch	quadratic mean canopy height profile (Lefsky et al., 1999)
medH	median of the canopy height (Lefsky et al., 1999)
centroid	height of the waveform centroids (Lefsky et al., 1999)
h_{14}	distance from signal beginning and ground peak, directly from GLA14
h_{100}	distance from signal beginning and ground peak, calculated from GLA01 waveform
satndx	waveform saturation index, i.e. the number of within-canopy bins that have brightness values indicating the detector was saturated
ASTER GDEM slope	slope based on elevation Δ in a 3 × 3 GDEM window centered on the GLAS pulse.

limited to areas below 60° N; the ASTER DEMs cover nearly all terrestrial surfaces (Hayakawa, Oguchi, & Lin, 2008; Hengl & Reuter, 2011). GDEM V1 accuracy is claimed to be 20 m at 95% confidence in the vertical dimension and 30 m at 95% confidence in the horizontal dimension. For further reference, Toutin (2008) has provided detailed information about ASTER GDEM processing.

Our processing developed mosaics of regional blocks of data (>500 tiles) using IDL/ENVI software. Blocks were processed with ENVI's topographic modeler, calculating min/max slope within a 90 × 90 m window. Elevations <3 m and >6195 m were excluded from slope calculations. Limitations to using this data are analogous to those of SRTM as both report canopy elevations.

2.5. Landsat and MODIS land products for stratification

We used three different land cover maps to identify land cover types for stratification purposes within eco-regions of the boreal biome in North America and Eurasia. Land cover data for Canada was provided by the Earth Observations for Sustainable Development (EOSD) project, which generated a 25-m land cover map based on Landsat-7 Enhanced Thematic Mapper plus (ETM+) data (centered on year 2000, with images from 1999 to 2002) released in 2006. Trees in this classification were defined as vegetation having a capacity to grow to heights > 5 m, and user accuracy for conifer forests was reported to be 86% in western Canada (Wulder et al., 2008). We have successfully used these data in a previous study of forest biomass in Quebec (Boudreau et al., 2008).

In Alaska, we used the 30-m National Land Cover Data (NLCD) 2001 classification based on Landsat-5 Thematic Mapper (TM) and Landsat-7 ETM + data collected between 1999 and 2004, with a majority of the imagery between 1999 and 2002 (Selkowitz & Stehman, 2011). This provided a consistent, up-to-date land cover layer for the entire state. The NLCD land cover for Alaska is available through the Multi-Resolution Land Characteristics Consortium (MRLC). The MRLC purchased three dates of Landsat imagery for the entire U.S. and coordinated the production of a comprehensive NLCD land cover database (Homer et al., 2007). The MRLC consortium is specifically designed to meet the current needs of federal agencies for nationally consistent satellite remote sensing and land cover data. Similar to EOSD, forests in this classification were defined as having heights > 5 m. Overall, accuracy of the product for forest non-forest is 83.9% (standard error of 2.1%) (Selkowitz & Stehman, 2011).

For Eurasia, we adopted a similar approach for stratifying land cover. However, we used the International Geosphere Biosphere Program (IGBP) classification scheme from the 2004 500-m Moderate Resolution Imaging Spectroradiometer (MODIS) global land cover (MOD12Q1) data (Justice et al., 1998), instead of Landsat ETM + land cover maps to stratify cover types within sub-biome. The MOD12Q1 data contains 17 land cover types; five of which are forest defined as having heights > 2 m (Friedl et al., 2010). Discrepancies in the identification of forested area near the taiga–tundra transition zone among remote sensing data products have been noted; however, good agreement exists throughout the boreal forest regions of northern Eurasia when comparing GLC-2000, GLOBCOVER, and MODIS IGBP classifications (Herold, Mayaux, Woodcock, Baccini, & Schmullius, 2008; Pflugmacher et al., 2011). Overall, global accuracy of the product has been stated to be 74.2% (Friedl et al., 2010), and we used five of the forest classes plus woody savanna, which is a dominant cover type over much of far eastern Siberia and the higher latitudes of the North American boreal forest.

We updated the two land cover products with recent burned area extents. We used a combination of fire polygon data obtained from the Canadian Forest Service and Alaska DNR and supplemented these with MODIS MCD45 1 × 1 km burned area fire products as needed (Roy, Boschetti, & Justice, 2006). NRCan-CCRS–CFS in Canada have a program to use the MODIS burn mapping to prioritize areas for collection of Landsat (or SPOT) data to map the fires with greater spatial detail than that available from MODIS. MODIS data were used exclusively for the Eurasia portion of the boreal forest.

2.6. Methods to develop biomass models

2.6.1. Ecoregion stratification

For a consistent biome-level analysis, we evaluated land area associated with ecoregions contained within the boreal forest biome of North America and Eurasia. The boreal land area, and its component ecoregions, was defined by the World Wildlife Fund's (WWF) ecoregion map of the world (Olson et al., 2001). We used these ecoregions, along with satellite-based land cover data, to create land cover strata, whereby the same land cover falling in different ecoregions was distinguished as unique strata. This stratum designation allowed for further refinement of land cover data and provided a means of grouping ground plots and LiDAR data (Fig. 1). Airborne measurements in Alaska and field measurements in northern Siberia enabled us to extend our approach into these areas.

2.6.2. Geographic data layers

We have developed a data acquisition strategy to obtain our estimates of aboveground biomass and C for the boreal forest of North America and Eurasia. To evaluate the variance of biomass estimates our basic study design relies on the following sources of data: 1) existing ground sample plots from various regions coupled with measurements of aboveground biomass on ground plots co-located with specific GLAS pulses; 2) PALS and ALTM airborne LiDAR data acquired over ground sample plots, with additional airborne PALS and ALTM data acquired along selected GLAS orbits; 3) automated quality-screened L3c and L3f GLAS data for the boreal forests of North America — 930,400 pulses, automated quality-screened L2a and L3a GLAS data in Scandinavia and western Eurasia — 738,159 pulses, and automated quality-screened L3c and L3f GLAS data in eastern Eurasia — 1,768,539 pulses (using criteria provided in Table 2); 4) Landsat land cover product for Canada (EOSD product), Alaska (NLCD product for the US; 30-m resolution) and MODIS MOD12Q1 land cover products for Eurasia; 5) ASTER GDEM V1 (98% global coverage); and 6) WWF ecoregions. The resolutions and sources of these data are summarized in Table 3.

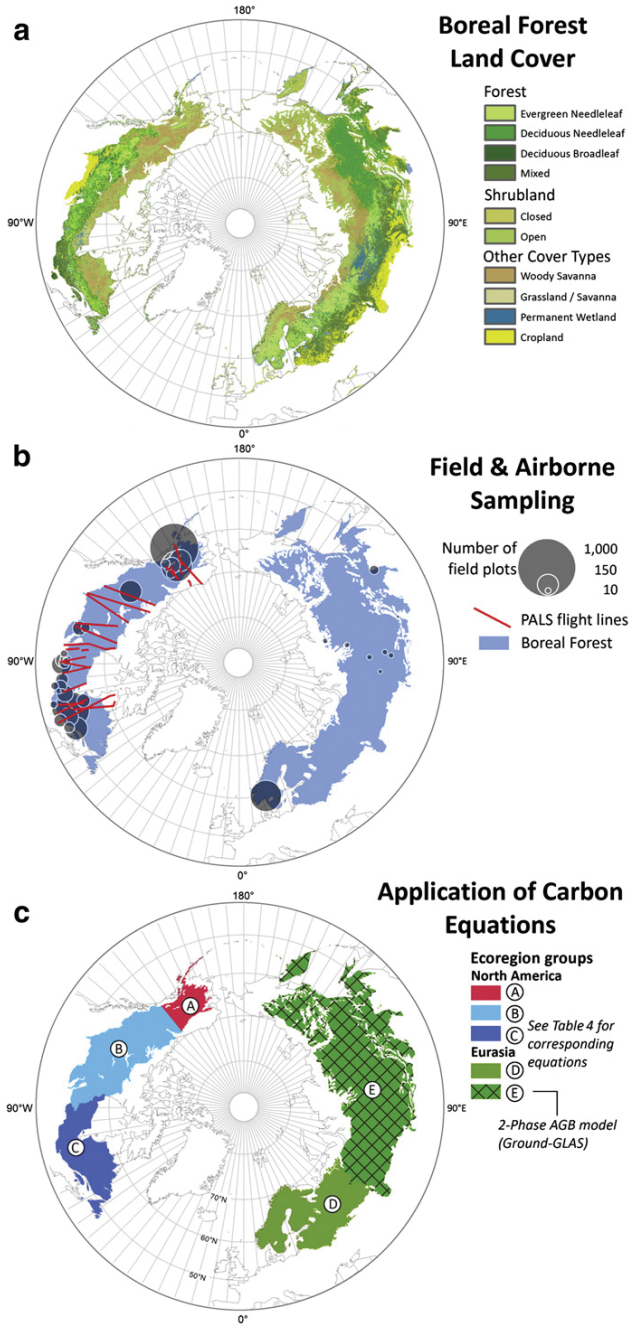

Fig. 1. Circumboreal forest stratification. a. Land cover information derived from MODIS and produced in the International Geosphere Biosphere Program classification scheme. b. The map shows the biomass sampling density throughout the study area with number of field plots shown by the size of gray circles. Red depicts portable airborne laser system (PALS) flight lines over co-located Geoscience Laser Altimeter System (GLAS) shots. c. A color-coded map depicting the regional spatial stratification of biomass models applied.

2.7. North America ground–PALS–GLAS sampling

The three-phase design used in North America involved: 1) flying PALS over existing USFS–FIA ground plots and the Canadian plots to develop models to relate ground-measured biomass to PALS metrics; 2) flying PALS along GLAS orbital tracks to measure profiling LiDAR height and canopy closure on individual GLAS pulses; and 3) developing a second set of models that relate PALS estimates of biomass to GLAS metrics. Once GLAS models for predicting forest biomass were calculated for the different land cover strata, the satellite LiDAR can be used as a sampling tool to attribute land cover strata across the continent.

Table 3
Data used to stratify study including source, resolution, and date.

Dataset	Source	Res. (m)	Date
MODIS MOD12Q1 (Eurasia)	http://reverb.echo.nasa.gov/	500	2004
MODIS MCD45	http://reverb.echo.nasa.gov/	1000	2003–06
ASTER GDEM V1	http://reverb.echo.nasa.gov/	30	2000–09
Landsat MLRC (Alaska)	http://www.mrlc.gov/	30	2001
Landsat EOSD (Canada)	http://tree.pfc.forestry.ca/	25	2000
WWF ecoregions	http://worldwildlife.org/publications/terrestrial-ecoregions-of-the-world	1000[a]	2000

[a] Minimum mapping unit applied after conversion from a vector ArcGIS shapefile.

2.8. Model based biomass estimation

The models reported below are similar to those reported by Nelson et al. (2012) and Ståhl et al. (2011). More information concerning the formulation of these models can be found in those references. In our design, we use the models below in a three-phase design in North America and western Eurasia (ground–airborne-GLAS with PALS and ALTM airborne LiDAR) and a two-phase design (ground–GLAS) in eastern Eurasia. An estimator of the mean value $\hat{\mu}_{Yc}$ (e.g., biomass, in Mg ha^{-1}) in stratum c is:

$$\hat{\mu}_{Yc} = \frac{\frac{1}{m}\sum_{i=1}^{m} G_{ic}(\hat{\alpha}_c)}{\frac{1}{m}\sum_{i=1}^{m} n_{ic}} \quad (1)$$

where $G_{ic}(\hat{\alpha}_c)$ is the total of all the per-hectare biomass estimates on GLAS shots that intercept stratum c along GLAS orbit i, where m is the number of GLAS orbits crossing that area of interest, and n_{ic} equals the number of GLAS shots intercepting stratum c on orbit i.

The mean per-hectare biomass across all C strata, can then be multiplied by the known total area to obtain an overall total which is:

$$\hat{\mu}_Y = \sum_{c=1}^{c} W_c \hat{\mu}_{Yc} \quad (2)$$

where W_c is the GIS-based area proportion of stratum c and $\sum_{c=1}^{c} W_c = 1.0$.

The variance of this total can be estimated as follows:

$$\hat{V}(\hat{\mu}) = \frac{1}{m}\sum_{c=1}^{c}\sum_{d=1}^{c}\frac{W_c W_d}{\overline{n}_c \overline{n}_d}\frac{\sum_{i=1}^{m}(G_{ic}(\hat{\alpha}_c)-\hat{\mu}_{Yc}n_{ic})(G_{id}(\hat{\alpha}_d)-\hat{\mu}_{Yd}n_{id})}{m-1} + \sum_{c=1}^{H}\sum_{d=1}^{H}\frac{W_c W_d}{\overline{n}_c \overline{n}_d}\sum_{j_1}^{p_c}\sum_{j_2}^{p_d} C\hat{o}v_{S2}\left(\hat{\alpha}_{j_1 c}, \hat{\alpha}_{j_2 d}\right)\widehat{G}_{j1c}\,\widehat{G}_{j_2 d} \quad (3)$$

where $\overline{n}_c$ is the denominator of model 1, i.e., the coverage number of GLAS shots that intercept stratum c on a given flight line. $C\hat{o}v_{S2}\left(\hat{\alpha}_{j_1 c}, \hat{\alpha}_{j_2 d}\right)$ is the covariance of the j_1 and j_2 coefficients in the

predictive model used to predict biomass in strata c and d, and p_c and p_d are the number of parameters, i.e., the number of independent variables, intercepts in the models used to predict biomass for strata c and d. $\hat{\widehat{G}}'_{j_1 c} = \frac{1}{m}\sum_{i}^{m}\sum_{t=1}^{T} g'_j(x_{it},\alpha)$ where $g'_j(x_{it},\alpha)$ is the value of the 1st derivative with respect to the jth coefficient of the predictive biomass model for the tth GLAS shot in the cth stratum, ith orbit.

The first term in model (3) describes sampling error; the second term (second line of model (3)) describes model error. Model error characterizes the variability of the coefficients of the predictive model(s) and describes how those coefficients and hence the predictive line or surface would change with repeated sampling. The model error in (3) does not describe prediction error, or the variability of a predicted biomass value around one specific prediction model. Prediction error could be added, as per Nelson et al. (2012), but it was not considered in this investigation.

Model (3) applies to situations where the models used to predict biomass in stratum c and d are: 1) dependent (e.g., different models developed using the same X, Y observations) and/or; 2) are one and the same, i.e., where the same model is used to estimate biomass in more than one cover class. If, as in the current study, models are developed independently, then the second term in Eq. (3) simplifies to the following:

$$+\sum_{c=1}^{c}\frac{W_c^2}{\overline{n}_c^2}\sum_{j_1}^{p_c}\sum_{j_2}^{p_c} C\hat{o}v\left(\hat{\alpha}_{j_1 c},\hat{\alpha}_{j_2 c}\right)\,\widehat{\widehat{G}}'_{j_1 c}\,\widehat{\widehat{G}}'_{j_2 c}.$$

For an individual stratum, the variance estimator is:

$$\widehat{V}(\hat{\mu}_{Yc}) = \frac{1}{\overline{n}_c^2}\frac{\sum_{i=1}^{m}(G_{ic}(\widehat{\alpha}_c) - \hat{\mu}_{Yc}n_{ic})^2}{m(m-1)} + \frac{1}{\overline{n}_c^2}\sum_{j_1}^{p_c}\sum_{j_2}^{p_c} C\hat{o}v\left(\hat{\alpha}_{j_1 c},\hat{\alpha}_{j_2 c}\right)\,\widehat{\widehat{G}}'_{j_1 c}\,\widehat{\widehat{G}}'_{j_2 c}. \quad (4)$$

3. Results

3.1. AGB models

To use GLAS as a sampling tool to estimate C, predictive models must be developed relating GLAS heights to ground measurements of AGB density. For the purposes of reporting results of total C mass and density, we divided our AGB model estimates by 50% (Houghton et al., 2000). In North America, an airborne LiDAR profiler was flown over existing ground plots where AGB had been measured as well as along ~15,000 km of GLAS orbits from Alaska to Quebec. We developed two sets of models, the first relating ground-measured AGB to airborne LiDAR height and canopy density metrics, and the second set relating airborne LiDAR estimates of AGB to GLAS metrics — a three-phase design. Western Eurasia followed a similar three-phase design, which employed an airborne LiDAR scanner in place of the profiler. GLAS footprints and field plots were overflown with ALTM on an area in southern Norway. The ground, airborne LiDAR, and GLAS measurements were used to formulate the models needed to generate biomass predictions for western Eurasia. Eastern Eurasia employed a two-phase approach relating field measurements directly to the GLAS measurements without the airborne LiDAR intermediary.

AGB models were developed for five circumpolar regions and, within each region for selected ecozones, for up to five independent strata for North America including, wetlands, hardwood, conifer, mixedwood, and burned areas. Two independent strata in western Eurasia were identified — conifer and hardwoods. In eastern Eurasia, we applied one generic model to all five strata due to the limited number of field plots in each of the strata. To develop these predictive models, we attributed every co-located GLAS footprint with data layers. We analyzed all possible subsets of GLAS metrics to identify those independent GLAS variables that best predicted AGB estimates based on LiDAR profiler measurements in North America, LiDAR scanner measurements in western Eurasia, and field measurements in eastern Eurasia. Once AGB models were established, we applied them to GLAS pulses by region, ecozones, and strata to provide C estimates across the entire boreal forest. Table 4 summarizes the models with variable definitions by region, ecozones, and strata that were used to generate the AGB estimates.

3.2. AGB estimates

We mapped by stratum the spatial distribution and standard error of C across the boreal biome, excluding shrubs (Fig. 2). Shrubs were excluded for two reasons: 1) the lack of boreal shrub allometric models and plots located in shrub areas; and 2) the lack of sensitivity of GLAS to vegetation < 5 m in height (Nelson, 2010). We estimated total biome C mass to be 38.0 ± 3.1 Pg (petagrams) distributed across a forested region encompassing 11.9 M km^2. We report our C estimates by stratum in Table 5, within each of five general circumpolar regions including Alaska, western Canada, eastern Canada, western Eurasia (west of the Ural Mountains), and eastern Eurasia (east of and including the Urals). Mean C density for the entire boreal forest biome is 20.3 ± 1.7 Mg ha^{-1} (million grams per hectare), with eastern Eurasia reporting the largest per-hectare quantity, 22.7 ± 3.4 Mg ha^{-1}. The eastern Eurasia standard errors are large relative to the standard errors reported for the other four regions due to the approach we used to predict biomass. A two-phase sampling approach was employed in eastern Eurasia, an approach that entails the use of a "direct" ground–GLAS model that predicts ground-based estimates of biomass as a function of GLAS measurements. In the other four regions, an airborne LiDAR was used as an intermediary to tie ground-based biomass estimates to GLAS metrics. The variance calculations in these three-phase designs ignore the ground–airborne LiDAR component and only incorporate the airborne LiDAR–GLAS model variances. The ground–airborne LiDAR model component was not included because our model-based estimator is limited to two-phase scenarios; we do not know how to legitimately incorporate the second (in this case, ground–airborne LiDAR) model uncertainty. We include in our variance estimate that model uncertainty which we believe is the larger of the two, i.e., the airborne LiDAR–GLAS model. The within- and across-strata variances in the four regions that utilize a profiling or scanning LiDAR are therefore under-reported by an unknown amount.

Across the entire circumboreal biome, 53% of the total C mass is in conifer forest (20.1 ± 2.4 Pg), 37% is in mixedwood forest (14.1 ± 0.6 Pg), 5% is in hardwood forest (1.8 ± <0.1 Pg), 4% is in woody wetlands (1.6 ± 0.3 Pg), and 1% is in forest that burned between 2000 and 2005 (0.4 ± 0.1 Pg). We note the burned area reported here is underestimated relative to other studies in North America (Kasischke et al., 2011), resulting in comparatively low C estimates for the burned area strata.

3.3. How do these results compare with other C estimates?

We performed validation of C estimates through study intercomparison on a country basis for those that completely fall within the boreal biome. For Canada, we used data reported by the two Canadian inventory systems, CanFI and NFI, as a source of validation of our LiDAR-based C estimates. Within the managed forest area, we compared our estimates to those produced by the Carbon Budget Model of the Canadian Forest Sector (Kurz & Apps, 1999). In Scandinavia and Russia, validation was more problematic. For instance, Norway, prior to 2005, inventoried only its commercial forest and ignored significant stretches of mountain forest and northern forests that were not currently marketable. Russian Federation forest inventory information tends to be in the southern boreal zone (similar to Canada), dated, and driven by local forestry needs. Our study and the Food and

Table 4
Study region model equations predicting aboveground live dry biomass (AGB). We approximate carbon to be 50% of AGB (Houghton et al., 2000). Models were developed via a three-phase sampling approach linking ground to airborne to satellite (Ground–PALS–GLAS) or a by a two-phase sampling approach linking ground to satellite (Ground–GLAS). Approaches varied by region (Fig. 1) in order to produce the most robust multiple linear predictive models with existing data. WWF ecoregions were grouped based on number of ground plots available, R^2, RMSE, and VIFS < 10, except for western Eurasia (D) stratum four where condition index was <12. Number of ground plots co-located to airborne measurements, and airborne to co-located GLAS acquisitions shown as (n). When constructed, condition number was the primary tool to quantify multicollinearity; post-analysis suggests that multicollinearity may be an issue here. For most of the boreal biome, models were developed for GLAS acquisitions L3c and L3f because regression models improved using these data as compared to using L2a and L3a. The exception was in western Eurasia, where L2a and L3a data were used. The Norway site was flown only over L2a.

(A) Alaska WWF ecoregions						
	Ground–PALS model	WWF ecoregion ID	RMSE Mg ha^{-1}	R^2	VIF[f]	n
Cook Inlet–Copper Plateau[a]	$\hat{y}_p = 20.06\ (\overline{h}_a) - 11.38\ (h_{70}) - 4.12$	50601, 50603, or 50604	38.73	0.54	2.87	157
Interior Alaska–Yukon	$\hat{y}_p = 3.61\ (h_{95}) - 6.94\ (h_{90}) + 1.22\ (d_{60}) + 3.46$	50607	39.15	0.58	1.85	111
St. Elias and Coast	$\hat{y}_p = 34.15\ (h_{50}) + 7.88\ (h_{10}) - 5.51$	51101	19.50	0.80	1.33	52
Interior Mackenzie Delta	$\hat{y}_p = 12.28\ (h_{60}) + 17.05\ (h_{30}) + 17.08$	51111 or 51116	29.24	0.74	4.12	41
Stratum	PALS–GLAS model					
Wetlands	$\hat{y}_g = 4.48\ (h_{14}) - 6.27\ (h_{50}) - 2.10\ (f_{slope}) + 6.31\ (acq3) + 11.66$		15.06	0.56	1.97	283
Hardwoods	$\hat{y}_g = 5.28\ (h_{90}) - 4.34\ (h_{25}) + 15.95\ (acq3) + 37.16$		23.75	0.53	1.85	176
Conifer	$\hat{y}_g = 7.39\ (h_{90}) - 8.75\ (h_{50}) - 1.35\ (acq3) + 36.98$		20.00	0.55	1.94	345
Mixedwood	$\hat{y}_g = 4.54\ (\overline{h}_{qc}) + 2.45\ (h_{14}) + 18.96\ (acq3) + 5.76$		29.62	0.54	4.92	156
Burned[b]	$\hat{y}_g = -2.79\ (h_{wflen\_adj}) + 7.79\ (h_{90}) - 8.05\ (h_{25}) - 3.05\ (f_{slope}) + 16.22\ (acq3) + 16.30$		17.37	0.57	6.34	179
(B) Western Canada WWF ecoregions						
	Ground–PALS model	WWF ecoregion ID	RMSE Mg ha^{-1}	R^2	VIF[f]	n
Muskwa/Slave Lake[a]		50502, 50607, 50608, 50609, 50610, 50612, 50613, 50614, 50617, 50802, 51101, 51111, or 51116				
Conifer	$\hat{y}_p = 2.98\ (h_{90}) + 7.02\ (h_{10}) + 2.03$		32.40	0.64	1.19	184
Hardwood[c]	$\hat{y}_p = 8.52\ (h_{50}) - 0.50\ (d_{80}) + 37.12$		30.18	0.65	1.74	51
Mixedwood	$\hat{y}_p = 12.70\ (\overline{h}_c) - 1.39\ (d_{80}) + 28.90$		35.23	0.64	1.70	35
All other cover types[e]	$\hat{y}_p = -6.23\ (\overline{h}_a) + 10.76\ (h_{10}) - 2.06$		22.22	0.84	5.74	36
(C) Central and E. Canada WWF ecoregions						
	Ground–PALS model	WWF ecoregion ID	RMSE Mg ha^{-1}	R^2	VIF[f]	n
Central Shield Forest						
Conifer	$\hat{y}_p = 12.04\ (h_{20}) - 7.96\ (s_a) - 1.18$	50602 or 50616	22.21	0.80	2.15	60
Hardwood	$\hat{y}_p = 13.19\ (\overline{h}_{qc}) - 0.73\ (d_{80}) + 2.36$		25.96	0.56	2.10	41
Mixedwood	$\hat{y}_p = 7.03\ (h_{95}) + 0.22\ (d_{40}) - 10.15$		26.74	0.60	1.02	98
All other cover types[e]	$\hat{y}_p = -6.23\ (\overline{h}_a) + 10.76\ (h_{10}) - 2.06$		22.22	0.84	5.74	36
Eastern Transitional Forest						
Conifer	$\hat{y}_p = 10.68\ (h_{95}) - 14.50\ (s_c) + 3.83$	50406	37.05	0.56	2.24	29
Hardwood[c]	$\hat{y}_p = 8.52\ (h_{50}) - 0.50\ (d_{80}) + 37.12$		30.18	0.65	1.74	51
Mixedwood	$\hat{y}_p = 10.93\ (\overline{h}_a) - 0.24\ (d_{30}) + 0.32$		28.63	0.48	1.46	82
All other cover types[e]	$\hat{y}_p = -6.23\ (\overline{h}_a) + 10.76\ (h_{10}) - 2.06$		22.22	0.84	5.74	36
Quebec and Maritimes[a]						
Conifer	$\hat{y}_p = 4.90\ (h_{90}) + 6.30\ (h_{10}) - 0.19$	50605, 50606, or 50611	27.90	0.69	1.75	66
Hardwood[c]	$\hat{y}_p = 8.52\ (h_{50}) - 0.50\ (d_{80}) + 37.12$		30.18	0.65	1.74	51
Mixedwood	$\hat{y}_p = 7.75\ (h_{60}) - 0.42\ (d_{80}) + 43.65$		30.82	0.49	2.19	88
All other cover type[e]	$\hat{y}_p = -6.23\ (\overline{h}_a) + 10.76\ (h_{10}) - 2.06$		22.22	0.84	5.74	36
Stratum	Western Canada PALS–GLAS model					
Wetlands	$\hat{y}_g = 5.52\ (h_{14}) - 5.17\ (h_{50}) - 2.22\ (acq3) + 4.82$	50610, 50613, 50614, or 51116	22.23	0.52	1.94	1567
Hardwoods	$\hat{y}_g = 2.33\ (h_{wflen\_adj}) + 3.44\ (\overline{h}_{qc}) - 5.26\ (acq3) + 35.68$		27.58	0.63	3.12	779
Conifer	$\hat{y}_g = 5.31\ (h_{14}) - 4.19\ (h_{25}) + 4.03$		21.28	0.68	1.38	3042
Mixedwood	$\hat{y}_g = 4.11\ (\overline{h}_{qc}) + 2.26\ (h_{14}) - 2.50\ (h_{25}) + 20.61$		23.40	0.59	3.48	570
Burned[d]	$\hat{y}_g = 5.46\ (\overline{h}_{qc}) + 4.07\ (ht\_jr) + 22.77\ (acq3) + 5.05$		27.15	0.66	1.47	31

Stratum	Central/Eastern Canada PALS–GLAS model					
Wetlands	$\hat{y}_g = 6.08\ (h_{14}) - 1.29\ (f_{slope}) - 1.20$	50406, 50602, 50605, 50606, 50608,	9.93	0.76	1.36	1348
Hardwoods	$\hat{y}_g = 3.92\ (\overline{h}_{qc}) + 6.09\ (h_{90}) - 5.44\ (h_{25}) + 9.32$	50609, 50802, 50407, 50410, or 50416	26.40	0.79	3.91	96
Conifer	$\hat{y}_g = 2.27\ (h_{14}) + 5.54\ (h_{90}) - 9.13\ (h_{25}) + 2.40$		23.56	0.62	4.66	850
Mixedwood	$\hat{y}_g = 5.74\ (h_{14}) - 0.92\ (senergy) - 5.01\ (h_{25}) + 14.63$		21.48	0.70	2.03	999
Burned[d]	$\hat{y}_g = 5.46\ (\overline{h}_{qc}) + 4.07\ (ht\_jr) + 22.76\ (acq3) + 5.05$		27.15	0.66	1.47	31
D) Western Eurasia WWF ecoregions						
Sarmatic Mixed Forest, Scandinavian and Russian Taiga, and Scandinavian Birch[a]						
Stratum	Ground–ALTM model[g]	WWF ecoregion ID	RMSE (Obs. vs. Predicted)			
			Mg ha^{-1}	R^2	VIF[f]	n
Conifer (mature spruce, med–high prod. sites)	$\hat{y}_a = 11.2024\ (hf_{100})^{1.2671}\ (dl_{70})^{0.80195}$	80436, 80608, or 81110	32.44	0.86	1.07	51
Conifer (mature pine, med–high prod. sites)	$\hat{y}_a = 7.4764\ (\mathrm{cvl})^{0.8322}\ (\mathrm{hl}_{10})^{0.6037}\ (dl_{70})^{0.6693}$		18.22	0.88	7.21	47
Conifer (mature spruce/pine, poor prod. sites)	$\hat{y}_a = 1.6446\ (hf_{90})^{2.1359}\ (df_{10})^{1.3024}\ (hl_{50})^{-0.6529}\ (dl_{50})^{-0.3661}$		13.72	0.86	7.03	51
Conifer (young spruce/pine, all site types) [h]	$\hat{y}_a = 10.0093\ (hf_{80})^{2.6478}\ (df_0)^{1.5588}\ (df_{40})^{-0.5094}\ (hl_{90})^{-1.5818}$		15.51	0.91	25.32	52
Stratum	ALTM–GLAS model					
Conifer, W. Wetlands, and W. Savanna	$\hat{y}_w = 5.95\ (h_{90}) - 5.00\ (h_{25}) + 4.72$		33.61	0.46	2.65	212
Mixedwood and hardwoods	$\hat{y}_w = 8.84\ (h_{75}) - 5.09\ (h_{25}) - 7.03$		29.29	0.77	4.47	73
(E) Eastern Eurasia WWF Ecoregions						
Central and Eastern Eurasia, and East Siberia[a]						
Stratum	Ground–GLAS model	WWF ecoregion ID	RMSE			
			Mg ha^{-1}	R^2	VIF[f]	n
		80505, 80601, 80603, 80604, 80605, 80606, 80607, 80609, 80610, 80611, 80444, 80809, 80519, 80817, or 81105				
All cover types	$\hat{y}_e = 13.60\ (h_{75}) - 14.30\ (h_{25}) - 3.49$		58.47	0.60	1.80	55

Variable definitions:

- *Dependent variables*

$\hat{y}_p$ PALS estimates of total aboveground live dry biomass, in Mg ha^{-1}, a Ground–PALS linear model formulated by regressing ground estimates of biomass against PALS height and canopy density measurements.
$\hat{y}_g$ GLAS estimates of total aboveground live dry biomass, in Mg ha^{-1}, a PALS–GLAS linear model formulated by regressing PALS estimates of biomass against L3a and L3c GLAS measurements.
$\hat{y}_a$ ALTM estimates of total aboveground live dry biomass, in Mg ha^{-1}, Ground-ALTM log model linearized by taking the natural log of both sides of the model, formulated by regressing ln(biomass) against ALTM height and density measures and then back-transforming.
$\hat{y}_w$ GLAS estimates of total aboveground live dry biomass, in Mg ha^{-1}, a ALTM–GLAS linear model formulated by regressing ALTM estimates of biomass against L2a and L3a GLAS measurements.
$\hat{y}_e$ GLAS estimates of total aboveground dry biomass, in Mg ha^{-1}, a ground–GLAS linear model formulated by regressing ground estimates of biomass against L3c and L3f GLAS measurements.

- *Independent variables*
  - *PALS variables in ground–PALS models*

$\overline{h}_a, \overline{h}_c, \overline{h}_{qc}$ average height, all pulses; average height, canopy hits only (>1.3 m); quadratic mean height, canopy hits, respectively
$h_{10}, h_{20}, h_{30}, h_{50}, h_{60}, h_{70}, h_{90}, h_{95}$ 10th, 20th, … 25th, 90th, and 95th height percentiles of the first return canopy height distribution
$d_{30}, d_{40}, d_{60}, d_{80}$ the 60th percentile cumulative canopy density in percent. To calculate d_{60} on a plot or GLAS shot, (1) sort all pulses between 1.3 m and h_{95}, (2) divide this sorted array into 10 equal height bins, and (3) calculate the percentage of pulses included in an above a given height bin relative to the total number of pulses in the plot or GLAS shot. So d_0 = (# pulses above 1.3 m) / (n_a), where n_a is the total number of pulses in the plot or GLAS shot. If h_{95} = 21.3 m so that each vertical bin is 2.0 m, then d_{10} = percentage of pulses above 3.3 m (=1.3 + 2.0), and d_{90} = the percentage of pulses above 19.3 m (=1.3 + 9 (2.0))
s_a, s_c standard deviation of $\overline{h}_a, \overline{h}_c$, respectively.

- ALTM variables in ground ALTM models

$hf_{80}, hf_{90}, hf_{100}$ 80th, 90th, and 100th height percentiles of the first echo canopy height distribution
hl_{50}, hl_{70} 50th and 70th density percentiles of the last echo canopy height distribution
df_0, df_{10}, df_{40} relative cumulative canopy height densities above the 0th (2 m), 1st, and 4th vertical height layers of the first echo height distribution, respectively
dl_{50}, dl_{70} relative cumulative canopy height densities above the 5th (2 m) and 7th vertical height layers of the last echo height distribution, respectively
cvl coefficient of variation of the last echo height returns.

(continued on next page)

Table 4 (*continued*)

- GLAS variables in PALS–GLAS models, ALTM–GLAS models, and the ground–GLAS model	
$\overline{h}_{qc}$	quadratic mean height of the waveform, calculated as the square root [$\sum$ (normalized amplitude in a given canopy height bin) × (height of bin)^2]
h_{25}, h_{50}, h_{75}, h_{90}	20th, 50th, 75th, and 90th percentiles of the waveform heights; e.g., h_{75} is that distance from the height bin below which 75% of the total waveform energy resides to the center of the ground peak
h_{14}	top of tree height, signal start to ground peak, GLA14 product
h_{wyflen}	height of the waveform, signal start to signal end, GLA14 product
f_{slope}	front slope to surface energy ratio from waveform as calculated by Sun et al. (2008)
senergy	energy from the ground = 2* (area under the lower half of the ground peak)
acq3	dummy variable, 0 if l3c acquisition, 1 if l3f acquisition
h_{wyflen_adj}	h_{wyflen}–*lead*–*trail*, where *lead* (m) and *trail* are (m) defined by Lefsky et al. (2007)
ht_jr	height from signal start to the centroid position of whichever of the two lowest fitted Gaussian peaks has greater amplitude, as defined by Rosette, North, and Suarez (2008).
[a]	More than two ecoregions combined and the name may not reflect all ecoregions.
[b]	Alaska grass and shrubs model used for burned areas in all of Alaska.
[c]	Generic model across all Canadian ecoregions except for the central shield forest because of limited sample sizes in hardwoods.
[d]	Generic model used across all of Canada due to limited sample size.
[e]	Generic model used for barren/shrubs/wetlands/herbs across all of boreal Canada.
[f]	Models with > 2 independent variables the largest variance inflation factor is reported.
[g]	Log–log models applied.
[h]	Condition index = 11.86. A condition number larger than 30 has been proposed to indicate sever collinearity.

Agriculture Organization–Forest Resources Assessment (FAO–FRA) report total aboveground Pg of C for 2005 by country. Note that a majority of studies do not report aboveground C separately. Furthermore, we are unaware of any other biome-based C maps with which comparisons can be made. To facilitate comparison with other studies whose maps and estimates of C stocks are reported for broad administrative units, we have aggregated boreal C results to the country level.

The countries by which we summarize the boreal C totals are those countries that contain ecoregions that are part of the boreal biome. It is important to note, when comparing total C that there is a large variation in each study's estimate of forested area. We provide Table 6, comparing our estimates by country with those from other studies. We found the following differences between our estimates and FAO–FRA: Russian Federation 6.6%; Canada 28%; Estonia 50%; Latvia 50%; Finland <0.1%; Norway <0.1% and Sweden 10%. In all comparisons, GLAS-based estimates were less than or equal to FAO–FRA estimates.

4. Discussion

Our approach utilizes model-based estimators and a two- or three-phase statistical sampling procedure (Nelson et al., 2012; Ståhl et al., 2011) to estimate C in forests. This approach is the culmination of long-term research that has focused on accounting for, and when possible, mitigating a variety of sources of uncertainty. Sources of uncertainty, or variance, include sampling variability, model error (i.e., variability of the coefficients), and the covariability among strata across all GLAS orbits. An early airborne LiDAR sampling study in Delaware (Nelson, Short, & Valenti, 2004) used Line Intercept Sampling (LIS) techniques (Kaiser, 1983) to calculate land cover stratum estimates and variances. LIS assumes that the LiDAR flight lines are randomly allocated across the study site when in fact, they were systematically spaced. Subsequent work in Quebec (Nelson, Boudreau, et al., 2009) and Siberia (Nelson, Ranson, et al., 2009) (1) accounted for regression error, (2) took into account the co-variability between adjacent and near-adjacent flight lines, and (3) tried to mitigate the potential inflationary effect of treating a systematic sample as a random sample by introducing successive-difference variance estimators. In Hedmark County, Norway we (Næsset et al., 2011) and others (Gregoire et al., 2011; Ståhl et al., 2011) have further refined variance estimators in the context of sampling large areas with airborne LiDARs. Gregoire et al. (2011) report on a model-assisted design-based statistical approach which may be employed in situations where a sample of airborne LiDAR flight lines is collected in association with a probability-based ground sample, e.g., an array of national forest inventory plots. The technique set forth by Ståhl et al. (2011) does not require the presence or integration of a probability ground sample, making this model-based technique more amenable to assessment of remote, inaccessible areas that lack a design-based sample of ground plots such as the circumboreal areas targeted in this study. Eastern Eurasia had only one ground–GLAS model primarily because of limited field sampling, and in part because of the absence of any available airborne LiDAR. The large uncertainty in this region is evident in Fig. 2 with eastern Eurasia containing error that is excluded in the three-phase design. Errors for this region are two to three times as much as reported in the three-phase design. Future studies should integrate airborne with additional field data in remote areas of Siberia to reduce this error and develop a solution to account for model error in situations where two models are used in a three-phase design to estimate biomass.

Our circumboreal assessment combined multiple data products assembled at different points of time and across many scales. This aggregation of data introduces many sources of error, some of which we do not account for, and these errors may propagate in unknown ways.

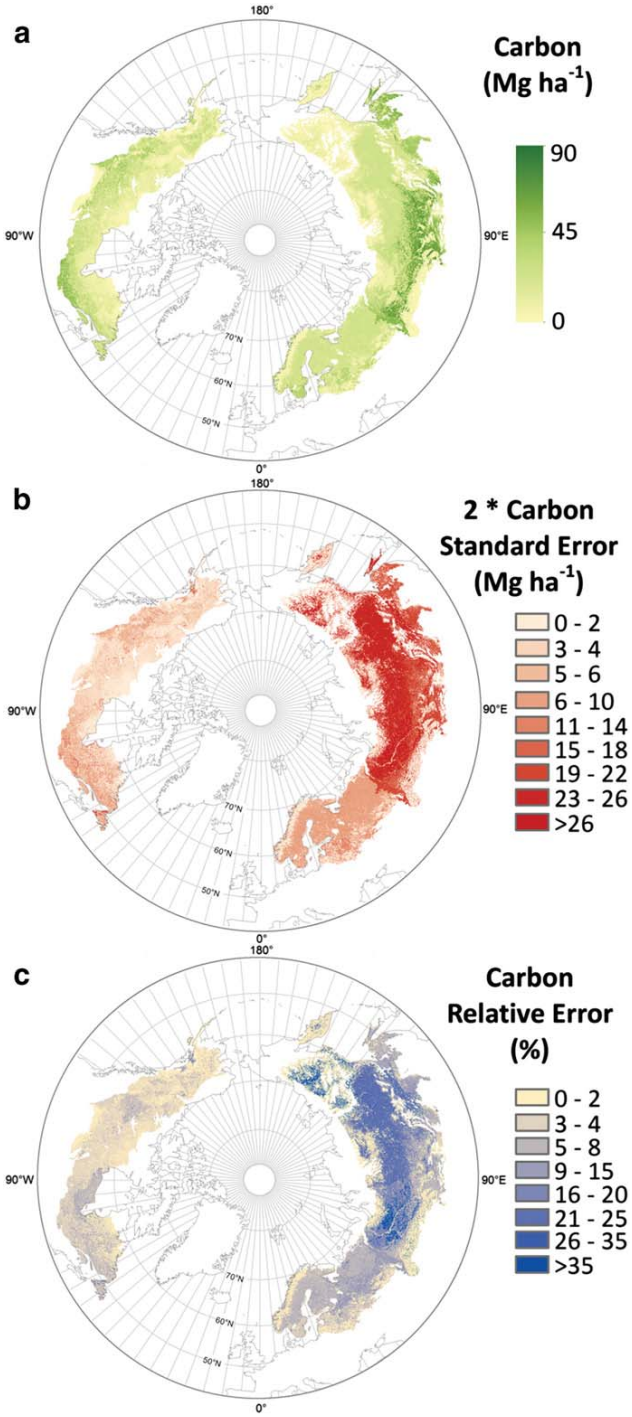

Fig. 2. Circumboreal forest. a, Aboveground carbon. b, c Error estimates of carbon density. The images illustrate stratum-level estimates reported in Table 5.

Sources of error that we believe could be better controlled, mitigated, or accounted for in future studies include:

1) temporal error associated to non-coincident ground, airborne, and GLAS measurements by land cover stratum — expected to be small in boreal forests, and larger for warmer, faster growing forests;
2) allometric error in models used to develop field plot biomass estimates — expected to be small in regional/national surveys (McRoberts & Westfall, accepted for publication);
3) geolocation error between ground plots and airborne LiDAR (5–15 m) — effect expected to be large as geolocation error exceeds 10 m (Gobakken & Næsset, 2009);
4) spaceborne LiDAR geolocation error (~15 m) — expected to be large;
5) land cover product geolocation error coupled with minimum mapping units, differences in forest height definition, and crown closure thresholds — unknown;
6) digital terrain model artifacts impacting slope calculations and geolocation errors — unknown; and
7) land cover product classification error. These sources of error we believe affected our results by an unknown amount. Future studies should consider these sources of error to improve C estimates — expected only to minimally result in regional across strata inaccuracy but it may result in assignment of biomass to incorrect strata.

These sources of error, we believe, affected our results by an unknown amount. Future studies should consider mitigating or accounting for these sources of error to improve C estimates.

Our study design, developed from prior investigations, imposed a sampling structure that we believe maximized utility of the products available to estimate circumboreal C. Using GLAS as our sampling tool, we characterize strata defined by publically available land cover maps. In Alaska, that was the 2001 30-m NLCD product that defines trees or forest as being vegetation that attain heights > 5 m (Gobakken & Næsset, 2009; Homer et al., 2007). In Canada, we employed the circa 2000 25-m EOSD product where forests were defined as vegetation with a capacity to grow > 5 m (Wulder & Nelson, 2003). In Eurasia, lacking wall-to-wall ETM + land cover maps, we employed the 2004 500-m MODIS MCD12Q1 IGBP product where forests were defined as vegetation > 2 m (Friedl et al., 2002). Future studies in Russia may find the hybrid land cover dataset useful as it provides more cover classes at higher resolution (Schepaschenko et al., 2011).

These land cover maps sources provide a stratification framework but do not limit the vegetation heights below which we cannot measure tree heights or estimate biomass with GLAS. Our vegetation height sensitivity is not driven by map definition; it is actually driven by the definition of tree used by the ground plot surveys. Typically, ground crews use minimum dbh and height limits to define what constitutes a tree. These dbh limits are approximately 5–10 cm, and 1.3 m in height in Norway for example (Ståhl et al., 2011). Depending upon the particular ground sample being discussed these minimum thresholds vary. GLAS is relatively insensitive to short sparse forest, but within our forested map strata as defined by the NLCD, EOSD, and MCD12Q1, we use GLAS nonetheless to estimate biomass across the entire height and density gradient. We purposely excluded non-forest strata, e.g. shrubs, water, shrub wetlands, that may in fact support some forest biomass and assume that if Landsat or MODIS identifies a particular GLAS shot as falling in the shrub stratum, then the biomass assigned to that GLAS shot is equivalent to zero, regardless of whatever vegetation height might have been measured by GLAS. We do this based on our experiences in Quebec, where GLAS "measured" significant biomass in areas that we knew were extensive areas of relatively flat rock, i.e. the Precambrian Shield in northern Quebec (Boudreau et al., 2008; Nelson, Boudreau, et al., 2009). By applying this approach, we believe that we probably miss significant amounts of forest biomass in areas defined by land cover maps as non-forest, but GLAS is not the appropriate tool to infer biomass in these areas.

Table 5
Aboveground C of the boreal forest, including sub-regions, and strata.

	North America			Eurasia		
	Alaska	W. Canada	E. Canada	West	East	Circumboreal
C by region						
Average density, Mg ha^{-1}	14.0	15.8	20.2	19.4	22.7	20.3
Standard error	0.3	0.3	0.8	1.0	3.4	1.7
Total biomass Pg	1.1	5.1	4.8	6.3	20.8	38.0
Standard error	<0.1	0.1	0.2	0.3	3.1	3.1
Area						Total area
Forest area, km^2 × 10^3	370.0	1779.6	1547.1	2350.4	5881.2	11,928.3
Non-forest area km^2 × 10^3	382.2	1433.3	820.4	891.3	3278.4	6805.6
Percent forest	49.2	55.4	65.4	72.5	64.2	63.7
Percent of boreal forest	4.0	17.2	12.6	17.3	48.9	100.0
Area by stratum, km^2 × 10^3						
Wetlands	58.7	480.7	300.2	79.0	331.4	1250.0
Hardwood	49.5	182.9	91.3	17.8	28.5	370.0
Conifer	205.9	921.2	780.9	1363.6	4011.7	7283.3
Mixedwood	45.8	163.7	365.0	887.4	1379.1	2841.0
Burned	10.2	31.1	9.7	2.5	130.6	184.1
C by stratum (Tg)						Total C
Wetlands	69.3	822.4	354.2	101.0	264.7	1611.6
Standard error	6.2	22.8	19.4	21.3	256.6	259.3
Hardwood	216.2	822.8	518.1	53.0	172.4	1782.5
Standard error	6.5	16.7	18.6	5.0	13.7	29.6
Conifer	579.6	2707.3	2310.9	3499.0	11,053.2	20,150.0
Standard error	13.7	64.6	162.9	251.4	2416.1	2435.5
Mixedwood	173.2	657.0	1568.0	2623.3	9041.1	14,062.6
Standard error	10.1	15.2	60.8	208.5	582.9	622.3
Burned	16.6	76.2	26.1	4.1	227.2	350.2
Standard error	1.3	9.8	4.8	1.4	89.9	90.6

5. Conclusions

Our circumpolar estimates of C, with standard errors, within the boreal forest build on the approaches above, and thus represent a significant advance in terrestrial C accounting. Furthermore, the sampling approaches and statistical analyses that we used provide important guidance to design and use of future spaceborne LiDAR systems for statistically evaluating terrestrial aboveground C stocks. The ICESat-2 photon-counting LiDAR, due for launch in 2016, and the recently approved BIOMASS satellite mission using P-band (435 MHz) SAR (Le Toan et al., 2011) could aid in re-measuring the circumboreal forest. (We note that the ability to collect P-band radar data over Europe and North America is currently not permitted at this frequency due to military restrictions; de Selding, 2013. The launch of BIOMASS is not planned until 2020, with the topic currently under high-level discussion — the outcome of which will affect boreal C mapping interests and initiatives). In general, these new systems and measures are desired to decrease the uncertainty around current estimates and to aid in assessing whether C management activities aiming to increase C stocks have indeed had a measurable large-area impact. Spaceborne LiDAR also has the potential to serve as a monitoring tool for quantitatively assessing how aboveground C stocks will vary with the large changes in climate predicted for northern regions (Soja et al., 2007).

Future monitoring of boreal C stocks will evolve with next-generation, space-based LiDAR instruments to produce a time series of C inventories. These time-series will provide insight to the spatial and temporal distribution of the changes in forest C stocks, and will enhance our ability to model and monitor the C cycle. For present modeling studies, the numbers reported here, with error bars, will place an important constraint on aboveground C pools that historically have been an under-constrained modeling problem. Understanding C changes resulting from forest management activities, climate change, or modification in the rates or intensity of harvest is critical to meet United Nations climate change treaty reporting goals.

Acknowledgments

This study was made possible by NASA's Terrestrial Ecology program under grants NNH08ZDA001N-TE and NNH06ZDA001N-CARBON. We also acknowledge the NSERC Discovery Grant to Hank Margolis for contributing partial support for the airborne data collection in Canada. We would like to thank three anonymous reviewers who improved the quality and content of this manuscript. We would also like to thank Sergi Im, Mukhtar Naurzbaev, Pasha Oskorbin, and Marsha Dvinskaya of the Sukachev Institute of Forest and Bruce Cook from the NASA Goddard Space Flight Center for help in collecting field measurements in Siberia.

References

Abshire, J. B., Sun, X. L., Riris, H., Sirota, J. M., McGarry, J. F., Palm, S., et al. (2005). Geoscience Laser Altimeter System (GLAS) on the ICESat mission: On-orbit measurement performance. *Geophysical Research Letters, 32*.

Alexeyev, V. A., & Birdsey, R. A. (1998). Carbon storage in forests and peatlands of Russia. *General Technical Report, NE-244, USDA Forest Service*.

Baccini, A., Goetz, S. J., Walker, W. S., Laporte, N. T., Sun, M., Sulla-Menashe, D., et al. (2012). Estimated carbon dioxide emissions from tropical deforestation improved by carbon-density maps. *Nature Climate Change, 2*, 182–185.

Botkin, D. B., & Simpson, L. G. (1990). The distribution of biomass in the North-American boreal forest. *Global Natural Resource Monitoring and Assessments: Preparing for the 21st century, Vols. 1–3.* (pp. 1036–1045).

Boudreau, J., Nelson, R. F., Margolis, H. A., Beaudoin, A., Guindon, L., & Kimes, D. S. (2008). Regional aboveground forest biomass using airborne and spaceborne LiDAR in Quebec. *Remote Sensing of Environment, 112*, 3876–3890.

Canadell, J. G., Pataki, D., Gifford, R., Houghton, R. A., Lou, Y., Raupach, M. R., et al. (2007). Saturation of the terrestrial carbon sink. In J. G. Canadell, D. Pataki, & L. Pitelka (Eds.), *Terrestrial ecosystems in a changing world* (pp. 59–78). Berlin: Springer-Verlag.

Table 6
Country comparison of boreal forest carbon (C) estimates. We report aboveground C ± 1 standard error.

Country	Forest area (10^6 ha^{-1})	Total C (Pg)	Standard error (Pg)	Mean C density (Mg ha^{-1})	Standard error (Mg ha^{-1})	Year	Source
Russian Federation							
	771.1	23.6	N/A	N/A	N/A	1990	Krankina and Dixon (1994)
	771.1	35.1	N/A	41.1	N/A	1990	Isaev, Korovin, Zamolodchikov, Utkin, and Pryaznikov (1995)
	886.6	22.1	N/A	N/A	N/A	1993	Krankina, Harmon, and Winjum (1996)
	882.0	28.0	N/A	36.3	N/A	1998	Alexeyev and Birdsey (1998)
	886.5	26.5[c]	N/A	38.6	N/A	1993	Shvidenko and Nilsson (2003)
	523.6[a]	23.1	N/A	44.1	N/A	2000	Houghton et al. (2007)
	826.6[a]	33.3	N/A	40.3	N/A	2000	Houghton et al. (2007)
	N/A	33.7[d]	N/A	N/A	N/A	1990	Goodale et al. (2002)
	642.2	24.4	N/A	38.0	N/A	1999	Dong et al. (2003)
	821.8	36.0	N/A	N/A	N/A	2000	Pan et al. (2011)
	845.6	37.5	N/A	N/A	N/A	2007	Pan et al. (2011)
	808.8	25.8[c]	N/A	N/A	N/A	2005	FAO–FRA[e]
	725.2	24.1	±3.1	33.2	4.2	2005	This study[f]
Canada							
	229.7	14.4	N/A	N/A	N/A	2000	Pan et al. (2011)
	229.4	14.0	N/A	N/A	N/A	2007	Pan et al. (2011)
	404.2	N/A	N/A	28.4[c]	N/A	1989	Kurz and Apps (1999)
	N/A	12.9[d]	N/A	N/A	N/A	1990	Goodale et al. (2002)
	512.6[g]	9.7[g]	±2.0[g]	19.0[g]	4.0	1990	Botkin and Simpson (1990)
	239.5	10.6	N/A	44.1	N/A	1999	Dong et al. (2003)
	310.1	13.7[c]	N/A	N/A	N/A	2005	FAO–FRA[e]
	332.7	9.9	±0.2	29.7[b]	0.6[b]	2005	This study
Estonia							
	2.3	0.1	N/A	47.5	N/A	1999	Dong et al. (2003)
	2.3	0.2[c]	N/A	N/A	N/A	2005	FAO–FRA[e]
	2.3	<0.1	<±0.1	23.3	3.0	2005	This study
Latvia							
	3.5	0.2	N/A	49.8	N/A	1999	Dong et al. (2003)
	3.3	0.2[c]	N/A	N/A	N/A	2005	FAO–FRA[e]
	2.8	0.1	<±0.1	41.8	3.6	2005	This study
Finland							
	17.2	0.6	N/A	34.9	N/A	1999	Dong et al. (2003)
	22.2	0.7[c]	N/A	N/A	N/A	2005	FAO–FRA[e]
	27.9	0.7	<±0.1	22.7	2.0	2005	This study
Norway							
	7.0	0.3	N/A	37.2	N/A	1999	Dong et al. (2003)
	9.7	0.3[c]	N/A	N/A	N/A	2005	FAO–FRA[e]
	10.7	0.3	<±0.1	29.8	1.6	2005	This study
Sweden							
	26.5	1.1	N/A	39.9	N/A	1999	Dong et al. (2003)
	28.2	1.0[c]	N/A	N/A	N/A	2005	FAO–FRA[e]
	33.1	0.9	±0.1	27.3	1.7	2005	This study

[a] Estimate of forest area from MODIS MOD12Q1 and GLC2000 land cover datasets.
[b] C and standard error estimated as mean between East and West Canada World Wildlife Fund (WWF) ecozones.
[c] C reported as living aboveground only biomass.
[d] Live vegetation C reported with understory.
[e] Food and Agriculture Organization Forest Resources Assessment (FAO–FRA) derived from 2005 database available online at: countrystat.org.
[f] Our Russian Federation forest area estimate is boreal only. We did not include non-boreal forests in the southeast or southwest.
[g] Values reported for all of boreal North America including Alaska.

de Selding, P. B. (2013). ESA to develop biomass mission despite operational, funding challenges. *SpaceNews*.

Dixon, R. K., Brown, S., Houghton, R. A., Solomon, A. M., Trexler, M. C., & Wisniewski, J. (1994). Carbon pools of global forest ecosystems. *Science*, *263*, 185–190.

Dong, J., Kaufmann, R. K., Myneni, R. B., Tucker, C. J., Kauppi, P. E., Liski, J., et al. (2003). Remote sensing estimates of boreal and temperate forest woody biomass: Carbon pools, sources, and sinks. *Remote Sensing of Environment*, *84*, 393–410.

Dymond, C. C., Neilson, E. T., Stinson, G., Porter, K., MacLean, D. A., Gray, D. R., et al. (2010). Future spruce budworm outbreak may create a carbon source in eastern Canadian forests. *Ecosystems*, *13*, 917–931.

Friedl, M. A., McIver, D. K., Hodges, J. C. F., Zhang, X. Y., Muchoney, D., Strahler, A. H., et al. (2002). Global land cover mapping from MODIS: Algorithms and early results. *Remote Sensing of Environment*, *83*, 287–302.

Friedl, M. A., Sulla-Menashe, D., Tan, B., Schneider, A., Ramankutty, N., Sibley, A., et al. (2010). MODIS Collection 5 global land cover: Algorithm refinements and characterization of new datasets. *Remote Sensing of Environment*, *114*, 168–182.

Gobakken, T., & Næsset, E. (2009). Assessing effects of positioning errors and sample plot size on biophysical stand properties derived from airborne laser scanner data. *Canadian Journal of Forest Research-Revue Canadienne De Recherche Forestiere*, *39*, 1036–1052.

Goetz, S. J., Mack, M. C., Gurney, K. R., Randerson, J. T., & Houghton, R. A. (2007). Ecosystem responses to recent climate change and fire disturbance at northern high latitudes: Observations and model results contrasting northern Eurasia and North America. *Environmental Research Letters*, *2*.

Goodale, C. L., Apps, M. J., Birdsey, R. A., Field, C. B., Heath, L. S., Houghton, R. A., et al. (2002). Forest carbon sinks in the northern hemisphere. *Ecological Applications*, *12*.

Gregoire, T. G., Ståhl, G., Næsset, E., Gobakken, T., Nelson, R., & Holm, S. (2011). Model-assisted estimation of biomass in a LiDAR sample survey in Hedmark County, Norway. *Canadian Journal of Forest Research-Revue Canadienne De Recherche Forestiere, 41*, 83–95.

Grosse, G., Harden, J., Turetsky, M., McGuire, A. D., Camill, P., Tarnocai, C., et al. (2011). Vulnerability of high-latitude soil organic carbon in North America to disturbance. *Journal of Geophysical Research — Biogeosciences, 116*.

Hansen, J., Sato, M., Ruedy, R., Lo, K., Lea, D. W., & Medina-Elizade, M. (2006). Global temperature change. *Proceedings of the National Academy of Sciences of the United States of America, 103*, 14288–14293.

Hansen, M. C., Stehman, S. V., & Potapov, P. V. (2010). Quantification of global gross forest cover loss. *Proceedings of the National Academy of Sciences of the United States of America, 107*, 8650–8655.

Harding, D. J., & Carabajal, C. C. (2005). ICESat waveform measurements of within-footprint topographic relief and vegetation vertical structure. *Geophysical Research Letters, 32*, L21S10.

Hayakawa, Y. S., Oguchi, T., & Lin, Z. (2008). Comparison of new and existing global digital elevation models: ASTER G-DEM and SRTM-3. *Geophysical Research Letters, 35*.

Hengl, T., & Reuter, H. (2011). How accurate and usable is GDEM? A statistical assessment of GDEM using LiDAR data. *Geomorphometry 2011* (pp. 4). Redlands, CA: Geomorphometry.org

Herold, M., Mayaux, P., Woodcock, C. E., Baccini, A., & Schmullius, C. (2008). Some challenges in global land cover mapping: An assessment of agreement and accuracy in existing 1 km datasets. *Remote Sensing of Environment, 112*, 2538–2556.

Homer, C., Dewitz, J., Fry, J., Coan, M., Hossain, N., Larson, C., et al. (2007). Completion of the 2001 National Land Cover Database for the conterminous United States. *Photogrammetric Engineering and Remote Sensing, 73*, 337–341.

Houghton, R. A., Butman, D., Bunn, A. G., Krankina, O. N., Schlesinger, P., & Stone, T. A. (2007). Mapping Russian forest biomass with data from satellites and forest inventories. *Environmental Research Letters, 2*.

Houghton, R. A., Skole, D. L., Nobre, C. A., Hackler, J. L., Lawrence, K. T., & Chomentowski, W. H. (2000). Annual fluxes or carbon from deforestation and regrowth in the Brazilian Amazon. *Nature, 403*, 301–304.

Isaev, A., Korovin, G., Zamolodchikov, D., Utkin, A., & Pryaznikov, A. (1995). Carbon stock and deposition in phytomass of the Russian forests. *Water, Air, and Soil Pollution, 82*, 247–256.

Justice, C. O., Vermote, E., Townshend, J. R. G., Defries, R., Roy, D. P., Hall, D. K., et al. (1998). The Moderate Resolution Imaging Spectroradiometer (MODIS): Land remote sensing for global change research. *IEEE Transactions on Geoscience and Remote Sensing, 36*, 1228–1249.

Kaiser, L. (1983). Unbiased estimation in line-intercept sampling. *Biometrics, 39*, 965–976.

Kasischke, E. S., Loboda, T., Giglio, L., French, N. H. F., Hoy, E. E., de Jong, B., et al. (2011). Quantifying burned area for North American forests: Implications for direct reduction of carbon stocks. *Journal of Geophysical Research — Biogeosciences, 116*.

Kharuk, V. I., Ranson, K. J., & Dvinskaya, M. L. (2008). Wildfires dynamic in the larch dominance zone. *Geophysical Research Letters, 35*.

Kharuk, V. I., Ranson, K. J., Kozuhovskaya, A. G., Kondakov, Y. P., & Pestunov, I. A. (2004). NOAA/AVHRR satellite detection of Siberian silkmoth outbreaks in eastern Siberia. *International Journal of Remote Sensing, 25*, 5543–5555.

Krankina, O., & Dixon, R. K. (1994). Forest management options to conserve and sequester terrestrial carbon in the Russian Federation. *World Resource Review, 6*, 88–101.

Krankina, O. N., Harmon, M. E., & Winjum, J. K. (1996). Carbon storage and sequestration in the Russian forest sector. *Ambio, 25*, 284–288.

Kurz, W. A., & Apps, M. J. (1999). A 70-year retrospective analysis of carbon fluxes in the Canadian forest sector. *Ecological Applications, 9*, 526–547.

Kurz, W. A., Dymond, C. C., Stinson, G., Rampley, G. J., Neilson, E. T., Carroll, A. L., et al. (2008). Mountain pine beetle and forest carbon feedback to climate change. *Nature, 452*, 987–990.

Lambert, M. C., Ung, C. H., & Raulier, F. (2005). Canadian national tree aboveground biomass equations. *Canadian Journal of Forest Research-Revue Canadienne De Recherche Forestiere, 35*, 1996–2018.

Le Toan, T., Quegan, S., Davidson, M. W. J., Balzter, H., Paillou, P., Papathanassiou, K., et al. (2011). The BIOMASS mission: Mapping global forest biomass to better understand the terrestrial carbon cycle. *Remote Sensing of Environment, 115*, 2850–2860.

Lefsky, M. A. (2010). A global forest canopy height map from the Moderate Resolution Imaging Spectroradiometer and the Geoscience Laser Altimeter System. *Geophysical Research Letters, 37*.

Lefsky, M. A., Harding, D., Cohen, W. B., Parker, G., & Shugart, H. H. (1999). Surface lidar remote sensing of basal area and biomass in deciduous forests of eastern Maryland, USA. *Remote Sensing of Environment, 67*, 83–98.

Lefsky, M., Harding, D., Parker, G., Acker, S., & Gower, S. (2002). LiDAR remote sensing of above-ground biomass in three biomes. *Global Ecology and Biogeography, 11*, 393–399.

Lefsky, M. A., Keller, M., Pang, Y., de Camargo, P. B., & Hunter, M. O. (2007). Revised method for forest canopy height estimation from Geoscience Laser Altimeter System waveforms. *Journal of Applied Remote Sensing, 1*.

Los, S. O., Rosette, J. A. B., Kljun, N., North, P. R. J., Chasmer, L., Suarez, J. C., et al. (2012). Vegetation height and cover fraction between 60A degrees S and 60A degrees N from ICESat GLAS data. *Geoscientific Model Development, 5*, 413–432.

McRoberts, R., & Westfall, J. A. (accepted for publication). The effects of uncertainty in model predictions of individual tree volume on large area volume estimates. *Forest Science* (accepted for publication).

Næsset, E., Gobakken, T., Solberg, S., Gregoire, T. G., Nelson, R., Ståhl, G., et al. (2011). Model-assisted regional forest biomass estimation using LiDAR and InSAR as auxiliary data: A case study from a boreal forest area. *Remote Sensing of Environment, 115*, 3599–3614.

Nelson, R. (2010). Model effects on GLAS-based regional estimates of forest biomass and carbon. *International Journal of Remote Sensing, 31*, 1359–1372.

Nelson, R., Boudreau, J., Gregoire, T. G., Margolis, H., Næsset, E., Gobakken, T., et al. (2009a). Estimating Quebec provincial forest resources using ICESat/GLAS. *Canadian Journal of Forest Research-Revue Canadienne De Recherche Forestiere, 39*, 862–881.

Nelson, R., Gobakken, T., Næsset, E., Gregoire, T. G., Ståhl, G., Holm, S., et al. (2012). Lidar sampling — Using an airborne profiler to estimate forest biomass in Hedmark County, Norway. *Remote Sensing of Environment, 123*, 563–578.

Nelson, R., Parker, G., & Hom, M. (2003). A portable airborne laser system for forest inventory. *Photogrammetric Engineering and Remote Sensing, 69*, 267–273.

Nelson, R., Ranson, K. J., Sun, G., Kimes, D. S., Kharuk, V., & Montesano, P. (2009b). Estimating Siberian timber volume using MODIS and ICESat/GLAS. *Remote Sensing of Environment, 113*, 691–701.

Nelson, R., Short, A., & Valenti, M. (2004). Measuring biomass and carbon in Delaware using an airborne profiling LIDAR. *Scandinavian Journal of Forest Research, 19*, 500–511.

Olson, D. M., Dinerstein, E., Wikramanayake, E. D., Burgess, N. D., Powell, G. V. N., Underwood, E. C., et al. (2001). Terrestrial ecoregions of the worlds: A new map of life on Earth. *Bioscience, 51*, 933–938.

Pan, Y. D., Birdsey, R. A., Fang, J. Y., Houghton, R., Kauppi, P. E., Kurz, W. A., et al. (2011). A large and persistent carbon sink in the world's forests. *Science, 333*, 988–993.

Pflugmacher, D., Krankina, O. N., Cohen, W. B., Friedl, M. A., Sulla-Menashe, D., Kennedy, R. E., et al. (2011). Comparison and assessment of coarse resolution land cover maps for Northern Eurasia. *Remote Sensing of Environment, 115*, 3539–3553.

Ranson, K. J., Sun, G., Kovacs, K., & Kharuk, V. I. (2004a). Landcover attributes from ICESat GLAS data in central Siberia. *IGARSS 2004: IEEE International Geoscience and Remote Sensing Symposium Proceedings, Vols. 1–7*. (pp. 753–756).

Ranson, K. J., Sun, G., Kovacs, K., & Kharuk, V. I. (2004b). Use of ICESat GLAS data for forest disturbance studies in central Siberia. *IGARSS 2004: IEEE International Geoscience and Remote Sensing Symposium Proceedings, Vols. 1–7*. (pp. 1936–1939).

Ropars, P., & Boudreau, S. (2012). Shrub expansion at the forest–tundra ecotone: Spatial heterogeneity linked to local topography. *Environmental Research Letters, 7*.

Rosette, J. A. B., North, P. R. J., & Suarez, J. C. (2008). Vegetation height estimates for a mixed temperate forest using satellite laser altimetry. *International Journal of Remote Sensing, 29*, 1475–1493.

Roy, D. P., Boschetti, L., & Justice, C. (2006). Global mapping of fire-affected areas using multitemporal MODIS data: The MCD45 product. *2006 IEEE International Geoscience and Remote Sensing Symposium, Vols. 1–8*. (pp. 4165–4168).

Saatchi, S. S., Harris, N. L., Brown, S., Lefsky, M., Mitchard, E. T. A., Salas, W., et al. (2011). Benchmark map of forest carbon stocks in tropical regions across three continents. *Proceedings of the National Academy of Sciences of the United States of America, 108*, 9899–9904.

Santoro, M., Beer, C., Cartus, O., Schmullius, C., Shvidenko, A., McCallum, I., et al. (2011). Retrieval of growing stock volume in boreal forest using hyper-temporal series of Envisat ASAR ScanSAR backscatter measurements. *Remote Sensing of Environment, 115*, 490–507.

Schepaschenko, D., McCallum, I., Shvidenko, A., Fritz, S., Kraxner, F., & Obersteiner, M. (2011). A new hybrid land cover dataset for Russia: A methodology for integrating statistics, remote sensing and in situ information. *Journal of Land Use Science, 6*, 245–259.

Selkowitz, D. J., & Stehman, S. V. (2011). Thematic accuracy of the National Land Cover Database (NLCD) 2001 land cover for Alaska. *Remote Sensing of Environment, 115*, 1401–1407.

Shvidenko, A., & Nilsson, S. (2003). A synthesis of the impact of Russian forests on the global carbon budget for 1961–1998. *Tellus Series B: Chemical and Physical Meteorology, 55*, 391–415.

Simard, M., Pinto, N., Fisher, J. B., & Baccini, A. (2011). Mapping forest canopy height globally with spaceborne LiDAR. *Journal of Geophysical Research — Biogeosciences, 116*.

Soja, A. J., Tchebakova, N. M., French, N. H. F., Flannigan, M. D., Shugart, H. H., Stocks, B. J., et al. (2007). Climate-induced boreal forest change: Predictions versus current observations. *Global and Planetary Change, 56*, 274–296.

Ståhl, G., Holm, S., Gregoire, T. G., Gobakken, T., Næsset, E., & Nelson, R. (2011). Model-based inference for biomass estimation in a LiDAR sample survey in Hedmark County, Norway. *Canadian Journal of Forest Research-Revue Canadienne De Recherche Forestiere, 41*, 96–107.

Stocks, B. J., Wotton, B. M., Flannigan, M. D., Fosberg, M. A., Cahoon, D. R., & Goldamer, J. G. (2001). Boreal forest fire regimes and climate change. *Remote Sensing and Climate Modeling: Synergies and Limitations, 7*, 233–246.

Sun, G., Ranson, K. J., Kimes, D. S., Blair, J. B., & Kovacs, K. (2008). Forest vertical structure from GLAS: An evaluation using LVIS and SRTM data. *Remote Sensing of Environment, 112*, 107–117.

Tarnocai, C., Canadell, J. G., Schuur, E. A. G., Kuhry, P., Mazhitova, G., & Zimov, S. (2009). Soil organic carbon pools in the northern circumpolar permafrost region. *Global Biogeochemical Cycles, 23*.

Tchebakova, N. M., Parfenova, E. I., & Soja, A. J. (2011). Climate change and climate-induced hot spots in forest shifts in central Siberia from observed data. *Regional Environmental Change, 11*, 817–827.

Toutin, T. (2008). ASTER DEMs for geomatic and geoscientific applications: A review. *International Journal of Remote Sensing, 29*, 1855–1875.

Wulder, M. A., Campbell, C., White, J. C., Flannigan, M., & Campbell, I. D. (2007). National circumstances in the international circumboreal community. *The Forestry Chronicle, 83*, 539–556.

Wulder, M. A., & Nelson, T. (2003). EOSD land cover classification legend report: Version 2. In C.F.S. Natural Resources Canada, Pacific Forestry Centre (Ed.), Victoria, British Columbia, Canada: CFS.

Wulder, M. A., White, J. C., Cranny, M., Hall, R. J., Luther, J. E., Beaudoin, A., et al. (2008). Monitoring Canada's forests. Part 1: Completion of the EOSD land cover project. *Canadian Journal of Remote Sensing, 34*, 549–562.

Yong, P., Sun, G. Q., & Li, Z. Y. (2004). Effects of forest spatial structure on large footprint LiDAR waveform. *IGARSS 2004: IEEE International Geoscience and Remote Sensing Symposium Proceedings, Vols. 1–7*. (pp. 4738–4741).